A 10-Gb/s Monolithically Integrated Filterless InGaAsP/InP Widely Tunable Wavelength Converter With Conversion Gain

Matthew N. Sysak, *Member, IEEE*, James W. Raring, *Member, IEEE*, Jonathon S. Barton, *Member, IEEE*, Henrik N. Poulsen, Daniel J. Blumenthal, *Fellow, IEEE*, and Larry A. Coldren, *Fellow, IEEE*

***Abstract*—In this paper, we present the details of a monolithically integrated filterless wavelength converter based on photocurrent-driven technology. The device consists of an integrated tunable laser transmitter and an optical receiver. The transmitter includes a sampled-grating distributed-Bragg-reflector laser, an electroabsorption modulator, and a semiconductor optical amplifier. The optical receiver employs two semiconductor optical amplifiers and a quantum-well p-i-n photodetector. The wavelength converter is characterized at 10 Gb/s over a variety of bias conditions at various input-power levels in various digital-system experiments. Bit-error-rate measurements at 10 Gb/s over an output tuning range of 32 nm between 1531 and 1563 nm show power penalties less than 1 dB. Similar experiments over an input wavelength range of 25 nm from 1535 to 1560 nm show a power penalty less than 2.5 dB. For a wavelength conversion from 1548 nm to a range of output wavelengths between 1531 and 1563 nm, the facet-to-facet gain ranges from 9 to 13 dB, neglecting fiber coupling losses.**

***Index Terms*—Monolithic integrated circuits, optoelectronic devices, wavelength conversion, wavelength-division multiplexing.**

I. Introduction

As BIT RATES and data-traffic levels scale in optical communication systems, dynamic wavelength management is viewed as critical to reduce blocking probabilities and provide an added flexibility to network architectures. Currently, dynamic wavelength switching is performed with the use of optical–electrical–optical (OEO) repeaters that are placed at high-traffic-network nodes. While these repeaters have been shown to be a viable solution at bit rates of up to 10 Gb/s and are currently moving toward 40 Gb/s, they suffer from a variety of drawbacks. Repeaters usually consist of several discrete components that have been copackaged together to perform wavelength management. Although this approach does allow for individual optimization of each discrete device, it suffers from inherent insertion-loss issues that occur when multiple components with different optimal optical-mode profiles are connected together. The narrow alignment tolerances that are created by these mismatched optical interfaces lead to complex packaging requirements that add cost and production time before the device can be brought to market. The other key drawback to the OEO repeaters is their inherent dependence on electronic circuit components. Particularly at high data rates, electronic circuit elements can be quite complex and require significant amounts of power [1].

As an alternative to using these OEO repeaters for wavelength-switching functionality, several monolithically integrated small-form-factor all-optical wavelength-switching elements have been proposed and demonstrated. Integrated devices that can combine several functionalities together on a single photonic chip offer significantly lower packaging costs with reduced power dissipation along with the potential for eliminating complex electronics. Examples of these integrated devices and the technologies that are utilized for wavelength switching include cross-gain and cross-phase modulation using optical amplifiers in interferometric structures [2], cross-absorption and photocurrent effects in electroabsorption modulators (EAMs) [3], photocurrent-based optical gates [4], and wave-mixing approaches in fiber and optical amplifiers [5]. In the case of the photocurrent-based optical gates, excellent switching performance has been demonstrated with extinction ratios (ERs) in excess of 10 dB and bit rates of up to 500 Gb/s.

Recently, several of these wavelength-switching elements have moved toward incorporating even more functionality onto a single small-form-factor device. Of particular interest in terms of adding new capabilities is an on-chip laser source [6]. Adding a laser to the integrated wavelength converter is attractive since it can reduce optical loss and potentially lower packaging costs. However, the integration of an on-chip laser source presents a new set of challenges. Previously, a filterless wavelength conversion using cross-absorption, cross-phase, and cross-gain effects simply mandated counterpropagating optical pump and data signals. With an integrated laser, this is more challenging since the stability of the optical source

Manuscript received August 1, 2006; revised May 4, 2007. This work was supported in part by DARPA/MTO CS-WDM under Grant N66001-02-C-8026 and in part by Intel Corporation under Grant TXA001630000.

M. N. Sysak is with the Ultrafast Optoelectronics Group, Department of Electrical and Computer Engineering, University of California—Santa Barbara, Santa Barbara, CA 93106 USA (e-mail: mnsysak@engineering.ucsb.edu).

J. W. Raring was with the Department of Materials, University of California, Santa Barbara, CA 93106 USA. He is now with the RF/Optoelectronic Group, Sandia National Laboratories, Albuquerque, NM 87185 USA (e-mail: jarring@engineering.ucsb.edu).

J. S. Barton is with the Department of Materials, University of California, Santa Barbara, CA 93106 USA (e-mail: jsbarton@ece.ucsb.edu).

H. N. Poulsen is with the Optical Communications and Photonics Network Group, Department of Electrical and Computer Engineering, University of California—Santa Barbara, Santa Barbara, CA 93106 USA (e-mail: Henrik@ece.ucsb.edu).

D. J. Blumenthal and L. A. Coldren are with the Department of Electrical and Computer Engineering, University of California—Santa Barbara, Santa Barbara, CA 93106 USA (e-mail: danb@ece.ucsb.edu; coldren@ece.ucsb.edu).

Digital Object Identifier 10.1109/JLT.2007.909333

requires tight control of any optical feedback. Several potential solutions to this issue have been proposed and demonstrated. These include cascaded wavelength converters, dual-order-mode approaches and multimode-interference (MMI)-based filtering [7], [8]. However, it has been difficult to demonstrate a fully transparent single-stage solution due to optical beating effects between the on-chip pump and data signals when wavelength switching is not desired [7].

As a solution to these filtering issues, a set of devices has been demonstrated using a photocurrent-driven approach where an on-chip optical receiver is used to drive a monolithically integrated EAM and tunable laser [9]. Similar to the other wavelength-conversion techniques, this device does not require electronics aside from a simple bias tee and a load resistor. However, the key benefit to this approach is that the optical input and output signals are physically separated from one another. This eliminates the possibility of optical interference between common wavelength input and converted signals. Furthermore, the integration of a tunable source allows for broadband wavelength conversion.

In this paper, we describe in detail the characterization and digital-switching performance of a monolithically integrated EAM-based photocurrent-driven wavelength converter (PD-WC). The device incorporates a widely tunable laser and a high-gain broadband optical receiver, which makes it ideal for wavelength switching with complete wavelength transparency with no optical filtering requirements regardless of input or output wavelength. Although this device has successfully been used for 2R ER regeneration and signal reamplification [10], and 3R regeneration including 2R regeneration with signal retiming [11], this paper focuses on the wavelength-switching aspects of the PD-WC without regeneration.

II. Device Overview

The PD-WC used in this paper consists of a monolithically integrated optical receiver and a tunable transmitter in a parallel-ridge architecture. A scanning-electron-micrograph (SEM) image, along with a functional schematic of the device, is shown in Fig. 1. The transmitter ridge includes a widely tunable sampled-grating distributed-Bragg-reflector (SGDBR) laser [12], a 550-μm semiconductor optical amplifier (SOA), and a 400-μm EAM. The receiver ridge contains a set of two SOAs and a 50-μm-long quantum-well (QW) p-i-n photodetector. The photodetector ridge width is linearly tapered from 12 to 3 μm for an increased saturation current while maintaining a relatively low capacitance. The first SOA is 600 μm long and 3 μm wide. The second SOA is 400 μm long and has an exponentially flared waveguide width (3–12 μm). This geometry enhances the 1-dB output-power compression of the amplifier, as described in Section IV-A of this paper. A Ti/Pt/Au metal line connects the photodetector and EAM contacts. A common dc bias is applied to both EAM and QW p-i-n through an external bias tee. The EAM and QW p-i-n share an electrical ground. A 50-Ω load resistor on the RF port of the bias tee sets the device bandwidth.

The wavelength-conversion process begins when light is coupled into the receiver waveguide and is amplified by the two

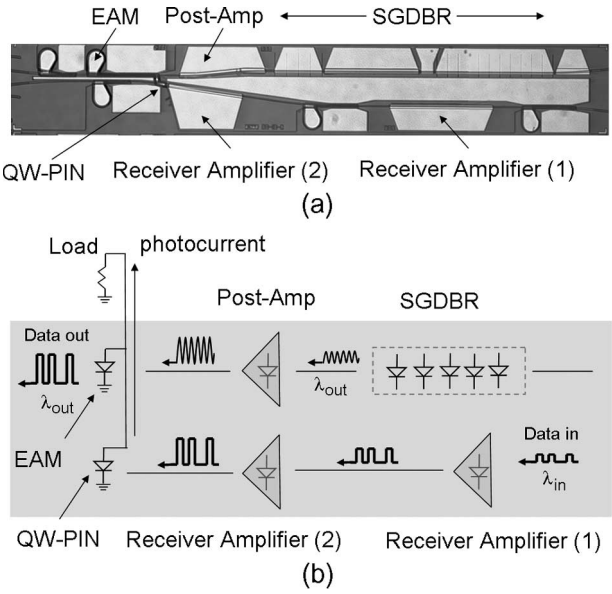

Fig. 1. (a) SEM of integrated PD-WC. The receiver section contains two SOAs and a QW p-i-n photodetector. The transmitter contains a widely tunable four-section SGDBR laser, a transmitter SOA, and an EAM. (b) Operating diagram of integrated PD-WC, including the details of the receiver amplification process and the wavelength-conversion process.

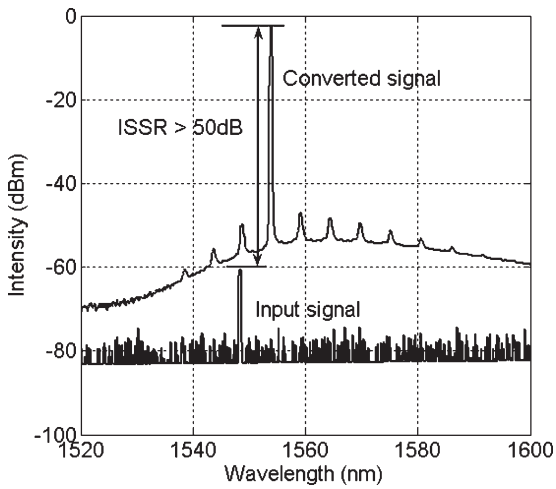

Fig. 2. ISSR for the PD-WC operating with an input fiber-coupled power of -11 dBm and an input wavelength of 1548 nm. The output wavelength is 1553 nm.

on-chip receiver SOAs. After the receiver SOAs, the amplified input is detected by the reverse-biased QW p-i-n photodetector. The 35-μm-long Ti/Pt/Au interconnect routes the amplified photocurrent signal from the photodetector to the EAM on the transmitter ridge and from the bias tee to the load resistor. The photocurrent drops across the load resistor, inducing a voltage change on the EAM. This voltage modulation changes the EAM transmission characteristics, thus transferring the input signal from the receiver to the output wavelength of the tunable laser.

To demonstrate the filtering characteristics of this device, a set of optical spectra from the output of the PD-WC was collected using an optical spectrum analyzer (OSA). The collected spectra are shown in Fig. 2. The "converted signal" data trace shows an output spectrum from the fully operational PD-WC tuned to an output wavelength of 1553 nm. In this case, the

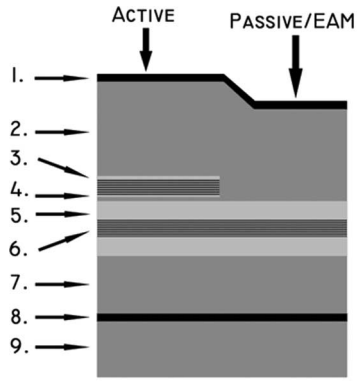

Region	Description
1	p-contact
2	p-cladding
3	Offset QWs
4	Stop Etch
5	Waveguide
6	Centered QWs
7	n-Buffer
8	n-contact
9	InP:Fe-substrate

Fig. 3. DQW integration platform with individual layer structure details.

receiver SOAs are biased at 6 kA/cm^2, both the QW p-i-n and EAM are biased at -2 V, and the SGDBR and postamplifier SOA are biased at 100 and 130 mA, respectively. For an input signal to the integrated receiver at 1548 nm with -11 dBm of fiber-coupled optical power, the output spectra from the PD-WC show no indication of the input signal. The small peaks in the converted signal are a result of the mirror reflectivity spectrum in the SGDBR laser.

For the "input signal" curve, the output from the wavelength converter is shown with the transmitter turned off but with the receiver amplifiers and QW p-i-n biased as in the "converted signal" case with the same input power (-11 dBm). The "input-signal" case represents the amount of light that manages to propagate from the input to the receiver then to the output lensed fiber that collects the wavelength-converted signal from the transmitter. Taking the ratio of the peak power from the PD-WC in the "converted signal" case to the peak power in the "input-signal" case gives the input-signal suppression ratio (ISSR). For the PD-WC, the results from Fig. 2 show an ISSR $>$ 50 dB.

III. Integration Platform

The wavelength converter is fabricated in the InP/InGaAsP material system using a dual-QW (DQW) integration platform [13]. A schematic of the epitaxial layers used in device fabrication is shown in Fig. 3. This platform is similar to the commonly used offset-QW (OQW) integration approach where a set of QWs above an optical waveguide region is used for optical gain and subsequently selectively removed to form the EAM and passive waveguide routing regions. The removal step is followed by a single metal–organic chemical vapor deposition InP regrowth over the entire wafer after which shallow ridges are patterned and etched.

In the DQW approach, the optical waveguide layer includes a second QW stack that has been shown to enhance modulation efficiency, increase device bandwidth, and reduce chirp of the integrated EAMs compared with the Franz–Keldysh modulators available on the OQW platform [14].

The OQWs above the waveguide layer consist of 7 $\times$ 6.5 nm compressively strained wells and 8 $\times$ 8 nm tensile-strained barriers. The photoluminescence (PL) peak is at 1550 nm. The waveguide QW stack consists of 7$\times$ 9 nm compressively strained wells and 6$\times$ 5 nm tensile-strained barriers with a PL peak of 1480 nm. The PL of the waveguide

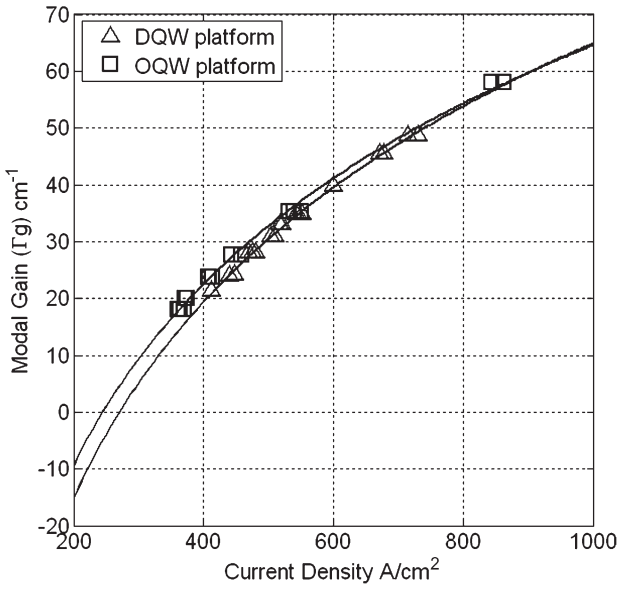

Fig. 4. Modal gain for OQW and DQW platforms. Results are from pulsed measurements of 50-μm-wide BALs.

wells has been selected to minimize the added optical loss that results from the Urbach tails of the waveguide and OQW stacks. The band offsets of the waveguide QWs are shallow to limit carrier screening effects in the reverse-biased EAM regions and to facilitate an efficient transport of the injected carriers through the waveguide region into the offset wells under forward-bias conditions. The upper and lower most 50 nm of the waveguide layer are Si-doped at 5×10^{16} cm^{-3}.

To measure the effect that the QW addition into the waveguide has on the laser performance, pulsed measurements of the differential efficiency and threshold current were performed on a set of DQW and OQW broad-area lasers (BALs) and narrow active ridge lasers (RL) using a cutback technique. These measurements were used to extract a material gain curve along with the laser injection efficiency. The OQW test lasers have a waveguide layer with a 1.4-μm bandgap and are uniformly doped 2×10^{17} cm^{-3} n-type with Si. The results from the DQW and OQW BAL test structures are shown in Fig. 4. Transparency current density and extracted material gain were 269 A/cm^2 and 764 cm^{-1}, respectively, for the DQW platform. For the OQW devices, the transparency current density was 246 A/cm^2, and the material gain was 826 cm^{-1}. Using the RL differential efficiency and threshold current data, the injection efficiencies were 73% and 75% for the OQW and DQW structures, respectively. The excellent agreement in the data between the two platforms indicates only minimal parasitic effects on the carrier transport properties for the active laser regions and optical amplifiers when adding the QWs into the waveguide.

The propagation loss has been measured for the DQW platform over a broad wavelength range using a long waveguide with identical periodic photocurrent monitoring structures. The loss is extracted as the ratio of the photocurrents at a fixed distance at each specific wavelength. The results for the wavelength-dependent loss are shown in Fig. 5. The exponential increase in the loss is consistent with what is expected from the Urbach tail of the waveguide QWs [15].

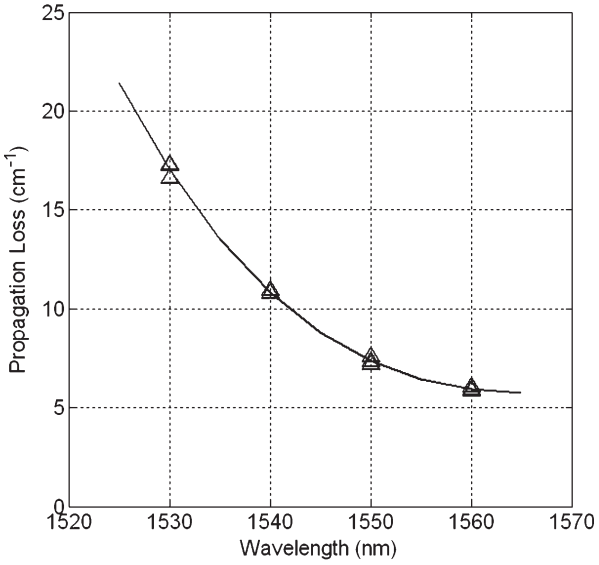

Fig. 5. Passive/EAM region propagation loss (units of per centimeter) at various operating wavelengths. Measurements were performed with integrated periodic tap structures.

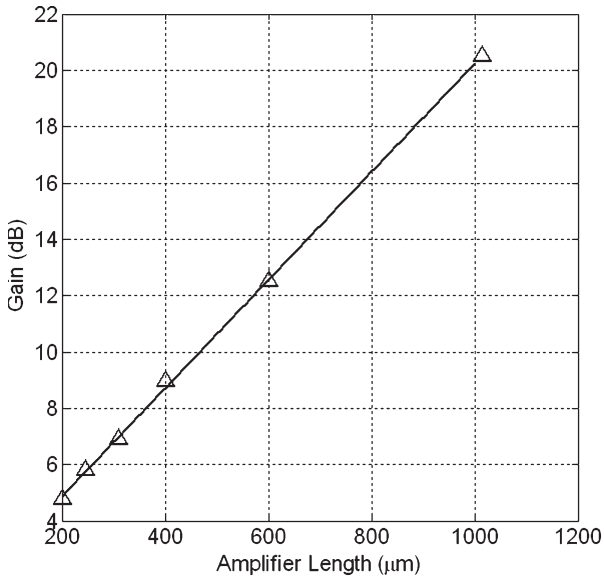

Fig. 6. SOA gain for 3-μm-wide ridge waveguide SOAs as a function of the device length for 1548 nm TE polarized input light. The applied current density is 6 kA/cm^2. A trend line is added to guide the eye.

IV. Integrated Receivers

The integrated wavelength-converter receiver consists of two SOA preamplifiers followed by a 50-μm QW p-i-n photodetector. The amplifiers and photodetector utilize the same OQWs as in the SGDBR laser gain and are either forward- or reverse-biased depending on whether gain or absorption is desired. Since the offset wells are compressively strained for optimal laser performance, the integrated receiver is polarization-sensitive with preferential gain for transverse electric (TE) guided modes. This issue could be circumvented by using a blanket growth and subsequent selective removal of a polarization-insensitive offset gain region, similar to that employed for unitraveling carrier photodetectors and low-confinement SOAs [16].

A. Integrated Optical Amplifiers

The two on-chip receiver SOAs are designed to amplify the input signal to the device before the QW p-i-n photodetector. For a highly linear and efficient design, this amplification process must be completed while simultaneously minimizing dissipated electrical power and avoiding optical saturation effects. To avoid optical saturation effects, the dimensions of the amplifiers are selected to keep the optical power at any point along each SOA at or below the 1-dB compression point. To minimize electrical power dissipation, the physical dimensions of the amplifiers are kept as small as possible without violating the optical saturation power requirements. This receiver is designed for a current density of 6 kA/cm^2. A plot of an amplifier gain as a function of the SOA length for 3-μm-wide amplifier is shown in Fig. 6. A plot of a measured and predicted amplifier output power as a function of the waveguide width and current density is shown in Fig. 7. The amplifier-gain predictions use a many-body-gain model described in [17].

The first SOA in the integrated receiver is 3 μm wide and 600 μm long. This amplifier width is selected to balance the

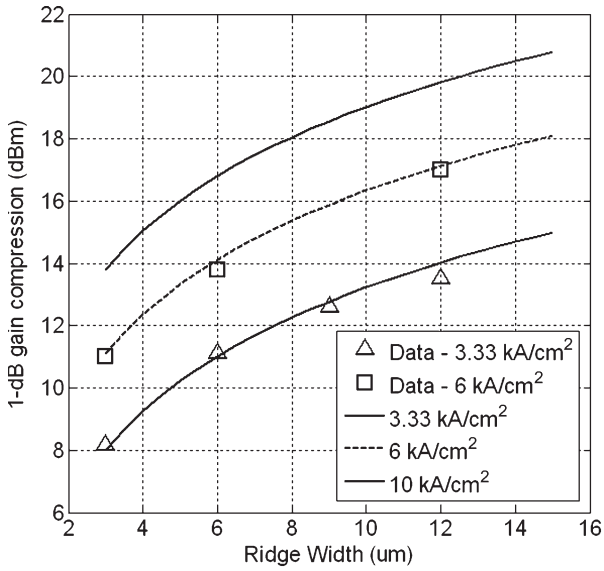

Fig. 7. Measured and simulated 1-dB gain-compression output powers for integrated receiver SOAs at an operating wavelength of 1548 nm with TE polarized light for various ridge widths and current densities.

waveguide propagation loss with the dissipated power. If the waveguide is too narrow, the propagation loss that results from a large modal overlap with the sidewalls becomes significant. The additional loss competes with the amplifier gain, and an increase in the total current (and hence electrical power) is required to compensate the waveguide sidewall effects, as shown in Fig. 7. However, if the waveguide is too wide, the physical dimensions of the device require a larger total current to achieve the same current density. The case of wide amplifiers is particularly problematic since the power dissipation varies as the product of the square of the applied current and the series resistance of the diode. It should be noted that wider amplifiers do have lower series resistance, but the decrease in resistance counteracts only one of the applied current terms, and the

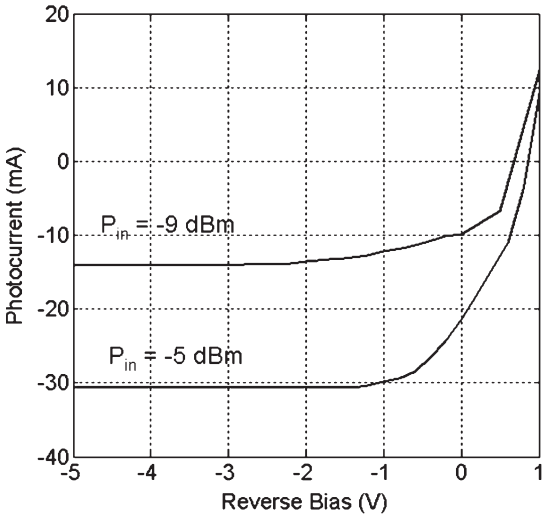

Fig. 8. Optically illuminated QW p-i-n IV characteristics. The input signal wavelength is 1548 nm, and the polarization is the TE. The receiver input-power levels are -9 and -5 dBm.

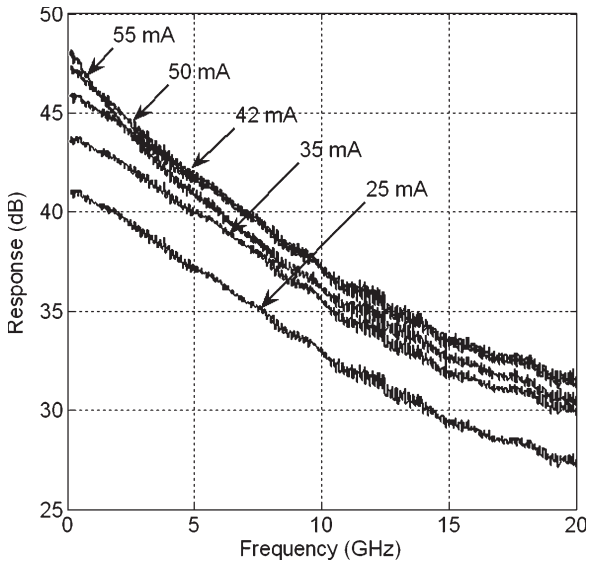

Fig. 9. Measured network-analyzer bandwidth and response of QW p-i-n photodetector test devices. Results show $>$ 42-mA average photocurrent without bandwidth degradation.

overall power dissipation still linearly scales with the amplifier width.

The measurements of the propagation loss show a sharp increase from 6 to 10 cm^{-1} at 1548 nm wavelength when the waveguide width is reduced from 3 to 2.5 μm. For the wider waveguides (5 μm), the propagation loss is only decreased from 6 to 5 cm^{-1} at the same wavelength. To keep the waveguide as small as possible without the introduction of an excess scattering loss, the waveguide width of the first amplifier is fixed at 3 μm.

The second receiver amplifier is 400 μm long and uses an exponentially flared waveguide width (from 3 to 12 μm) to allow the optical mode to laterally expand. As the modal cross-sectional area increases, the photon density in the OQW stack remains fixed, delaying the amplifier saturation effects and allowing the total waveguide power in the amplifier to increase beyond the 1-dB gain compression of a fixed width 3-μm-wide SOA. For a 12-μm-wide SOA, the output 1-dB gain compression is $+17$ dBm.

Given that the total length of the entire preamplifier is 1000 μm, the estimated gain for both integrated SOAs is 20.5 dB. It should be noted that although the results from the many-body-gain model shown in Fig. 7 predict further enhancements in the output-power gain compression, significant heating issues prevented the bias conditions from exceeding 6 kA/cm^2. Improvements such as in flip chip that is bonding the PD-WC and using a conducting substrate for low device resistance would provide significant improvements in terms of increasing the bias current to the receiver amplifiers.

B. Integrated QW p-i-n Photodetectors

The QW p-i-n photodetector consists of a reverse-biased region that contains the OQWs. The device is 50 μm long with a waveguide width that is linearly tapered from 12 to 3 μm.

Optically illuminated current–voltage $(I-V)$ characteristics for the integrated photodetector in the PD-WC receiver are shown in Fig. 8. For a CW signal that is fed into the receiver at 1548 nm and for the SOAs that are biased at 6 kA/cm^2, the QW p-i-n generates a uniform amount of photocurrent for the applied reverse-bias conditions increasing beyond approximately -1 V. This is an important characteristic since this allows the reverse bias applied to both the QW p-i-n and EAM to be selected independent of concerns for improving the QW p-i-n absorption efficiency. Eliminating these concerns makes it possible to select the bias of the wavelength converter based on the EAM efficiency optimization.

Although these devices can be highly absorbing at low bias, the QW p-i-n structures typically suffer from front-end saturation and carrier screening effects under high optical powers [18]. To counteract these effects, the wide-area detectors have been shown to reduce the optical photon density at the absorbing medium by spatially spreading the optical mode in a similar manner to what is employed for the on-chip receiver amplifiers. Using this technique in the standard OQW integration platform, the QW p-i-n photodetectors have previously demonstrated 10 Gb/s operation with output voltage swings of 0.8 V peak to peak across a 50-Ω load [19].

To investigate the properties of the wide-area DQW-platform QW p-i-n photodetectors, several test devices have been fabricated, which are 100 μm long and 12 μm wide. The results of the 50-Ω terminated S_{21} optical-to-electrical bandwidth as a function of the applied bias and detected photocurrent are shown in Fig. 9. Up to 42 mA of the average photocurrent can be accommodated in the QW p-i-n structures before the bandwidth of the device is degraded at an applied bias of -3 V.

C. Integrated Receiver

The fully integrated receiver dc gain, including both the SOA gain and the QW p-i-n quantum efficiency, is shown in Fig. 10 for a range of CW input powers at a wavelength of 1548 nm. The results show 20.1 dB of unsaturated optical gain at an applied current density of 6 kA/cm^2. The input- and output-power

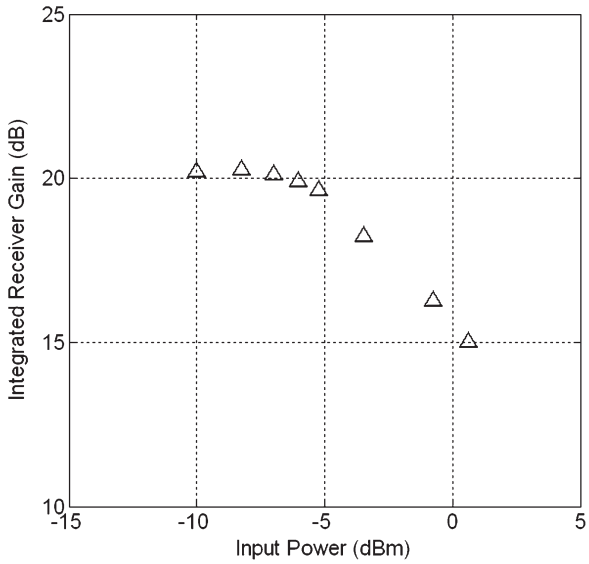

Fig. 10. Integrated wavelength-converter receiver dc gain including QW p-i-n and both receiver SOAs for 1548 nm TE polarized light. The receiver dc bias is -3 V, and the receiver amplifiers were biased at 6 kA/cm^2.

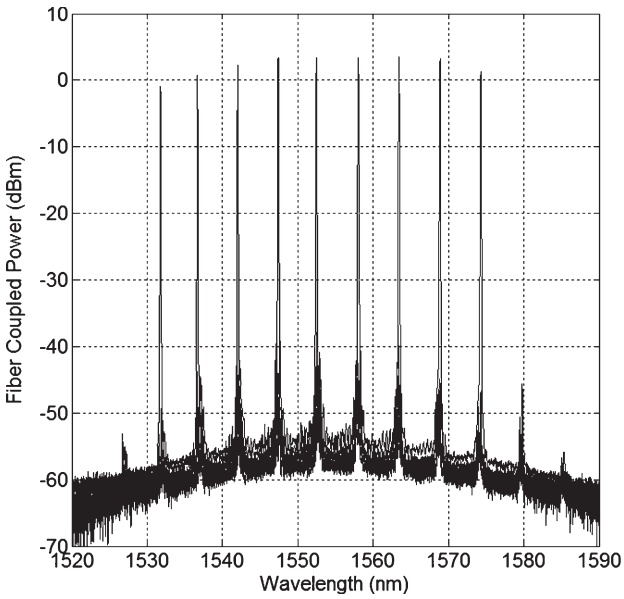

Fig. 11. Overlaid SGDBR fiber-coupled output spectra showing tuning from 1532 to 1575 nm and output powers from $+5$ to -3 dBm. Laser gain and SOA postamplifier are both biased at 100 mA. Fiber coupling loss is 4.2 dB.

levels, where the amplifier gain rolls off by 1 dB, are -4 and $+16.1$ dBm, respectively.

V. Integrated Transmitters

The transmitter section of the wavelength converter consists of a four-section widely tunable SGDBR laser along with a backside absorber, a 550-μm-long postamplifier SOA to boost the laser output power, and a 400-μm-long EAM. The overlaid transmitter output spectra, with the laser gain and SOA postamplifier biased at 100 mA each, are shown in Fig. 11. The fiber-coupled output-power levels range between $+5$ dBm at 1560 nm and -3 dBm at 1532 nm. The fiber coupling loss was

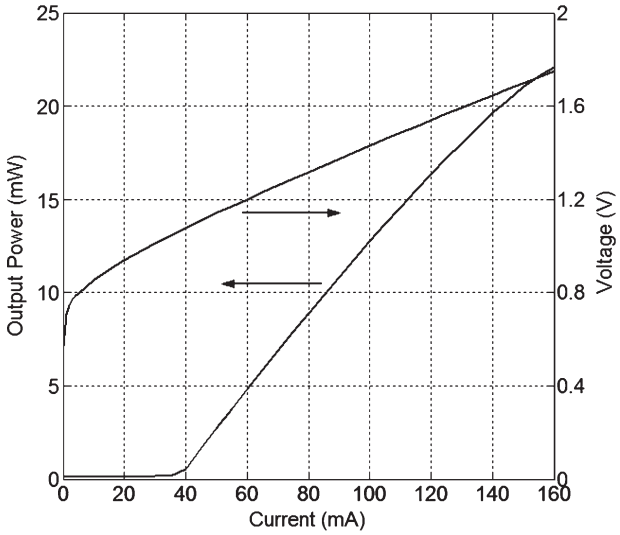

Fig. 12. SGDBR $I-V$ and light versus current characteristics measured into the reverse-biased postamplifier that follows the laser. The laser output wavelength is 1550 nm.

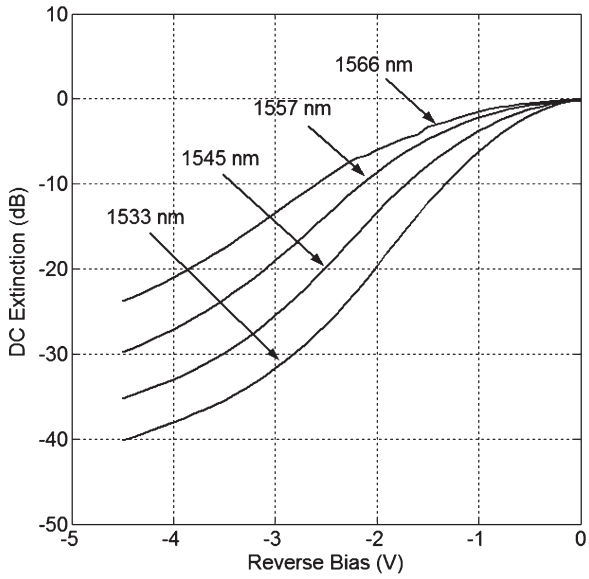

Fig. 13. Broadband dc extinction characteristics of 400-μm-long DQW EAM. Measurements are performed by tuning the SGDBR to the indicated wavelength and fiber coupling the output to an optical power meter.

4.2 dB. The on-chip light versus current and the IV characteristics from the SGDBR laser were measured by reverse biasing the postamplifier that follows the laser and are shown in Fig. 12. The SGDBR output power at 1550 nm is >20 mW with a gain bias on chip of 160 mA.

The EAM dc extinction and the slope efficiency over a range of wavelengths are shown in Figs. 13 and 14, respectively. For the 400-μm-long EAM, a greater than 8-dB/V slope efficiency is observed over a 30 nm wavelength range with an absolute extinction ranging from 25 to 45 dB at a reverse bias of -4.5 V.

The 50-Ω terminated S_{21} electrical-to-optical bandwidth of the 400 -μm-long EAM was 11 GHz and showed little variation with up to 17 mA of average photocurrent as discussed in [13].

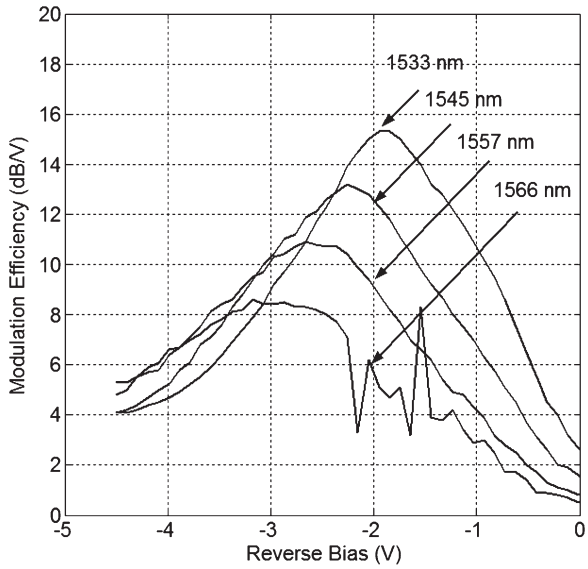

Fig. 14. Local slope efficiency $\mathrm{d}T/\mathrm{d}V$ (in decibels per volt) for the integrated DQW 400-μm-long EAM. Greater than 8 dB/V can be achieved at all output wavelengths at the appropriate dc-bias position.

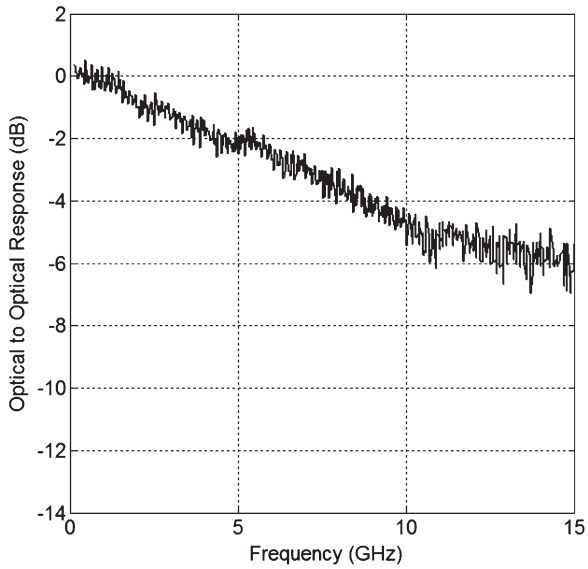

Fig. 15. Optical-to-optical S_{21} bandwidth measurements for the integrated PD-WC with an external 50-Ω termination. The input and output wavelengths are 1548 and 1555 nm, respectively.

VI. Dynamic Wavelength-Converter Measurements

The integrated wavelength converters described in Section II were thinned, cleaved into bars, antireflection (AR)-coated, wire-bonded, and mounted on copper studs for testing. For characterization of the PD-WCs, the receiver SOAs are biased at 6 kA/cm^2, and the laser gain and the transmitter postamplifier are biased at 130 and 100 mA, respectively.

The optical-to-optical 3-dB bandwidth of the 50-Ω terminated PD-WC was measured using a 20-GHz network analyzer for a conversion from 1548 to 1555 nm. The results can be seen in Fig. 15 and show a 3-dB bandwidth of approximately 7 GHz with a reverse bias of -2.5 V. Although not included in the plot, the bandwidth of the PD-WC is relatively insensitive to reverse-bias levels in excess of -1 V. The low-bias dependence is due to the low doping levels in both the EAM waveguide and the OQWs and to the high doping in the InP n-buffer layer (Fig. 3). Once the applied voltage is sufficient to deplete the EAM and QW p-i-n waveguides, the doping in the buffer (Si at 1×10^{18} cm^{-3}) prevents the depletion width in these components from increasing as the bias voltage is increased. The fixed depletion width clamps the depletion capacitance and preserves the RC time constant that controls the PD-WC bandwidth.

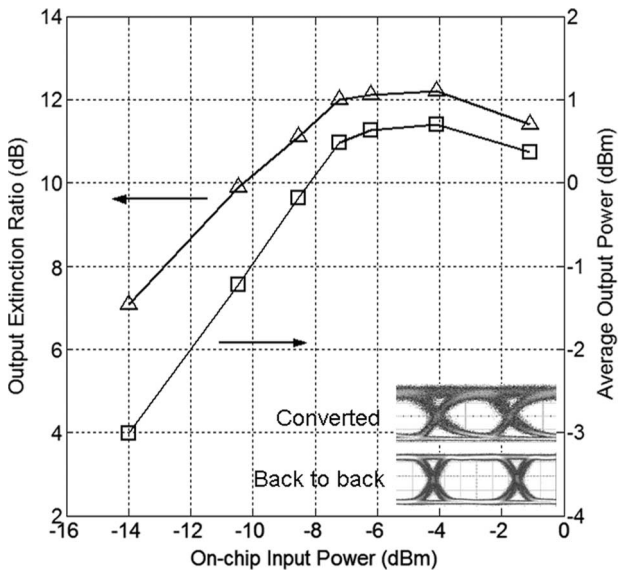

Fig. 16. Average fiber-coupled output power and ER for the integrated PD-WC as a function of the receiver input power. The applied reverse bias is -2.2 V, and the output wavelength is 1555 nm. The eye diagrams are for back-to-back and wavelength-converted signals with -7-dBm receiver input power.

To characterize the switching performance of the PD-WC, the receiver input power, the output wavelength, and the applied dc-bias conditions have been varied, and the wavelength-converted output-signal ER and output power have been measured. The converted ER is measured in the eye diagram where the separation between the "one" and "zero" levels is at a maximum. Characterization is performed with a 1548 nm input signal at 10 Gb/s using a $2^{31} - 1$ psuedorandom bit stream (PRBS). The light from an optical transmitter is fed through an erbium-doped fiber amplifier, an optical filter (0.35 nm), and a polarization controller before it is launched into the device using a lensed fiber. The output PD-WC extinction and output-power characteristics are measured by examining the fiber-coupled optical output into a component analyzer.

The effect that increasing the input power to the receiver has on the wavelength-converted extinction and average converted fiber-coupled output power is shown in Fig. 16. In this experiment, the reverse bias is -2.2V. The input wavelength is 1548 nm, and the output of the PD-WC is 1555 nm. The eye diagrams are included in the figure for the back-to-back and wavelength-converted signals with an input power of -7 dBm.

As the input power to the receiver increases, both the ER and the output power gradually improve and then level off at 12 dB and $+0.5$ dBm, respectively.

The shape of the ER response is due to a combination of EAM efficiency effects and receiver saturation effects. For low

input powers where the receiver SOAs can operate in their linear regime, the increases in the input power create corresponding increases in the photocurrent from the QW p-i-n and, hence, an increasing voltage over the load resistor. This increase in voltage generates larger swings in EAM transmission and results in larger PD-WC ERs.

However, as the input power to the receiver continues to increase, several factors begin to limit device performance. As voltage swings from the receiver get larger, the integrated EAM is driven well beyond the optimal slope efficiency point in Fig. 14. Under these conditions, even though the preamplified receiver is continuing to generate larger photocurrent levels, the reduced EAM efficiency leads to smaller incremental increases in the PD-WC extinction.

The other factor that plays an important role in the wavelength-converter extinction is the receiver preamplifier response (Fig. 10). As the input powers approach the amplifier saturation power, the optical gain from the receiver is degraded. Under these conditions, the shape of the amplified signal to the photodetector becomes distorted by the gain overshoot, and the photocurrent that is used to drive the integrated EAM adds significant noise to the converted signals, distorting the ER from the PD-WC.

The average output-power characteristics from the wavelength converter, which are shown in Fig. 16, are controlled by a combination of the EAM "OFF" state and slope efficiency. For low input powers, the output power from the PD-WC initially increases before finally rolling over due to the EAM slope-efficiency degradation and amplifier saturation. Since the extinction and the output power for the fixed-bias conditions used in Fig. 16 do not significantly improve beyond an input power of -7 dBm, further device characterization is performed at this input power.

In the next set of experiments, the wavelength-converter output-power and ER performance is characterized over a range of electrical bias voltages and over a range of output wavelengths using the -7 dBm input power. The results are shown in Figs. 17 and 18 for the wavelength-converted ERs and the average output powers, respectively. Over the output wavelengths ranging from 1533 to 1564 nm, greater than 10-dB extinction is achievable by setting the appropriate reverse-bias conditions. For a particular output wavelength, as the reverse bias is moved toward the bias conditions that correspond with the maximum EAM slope efficiency (Fig. 14), the output extinction is improved. However, as the bias is increased and the output extinction improves, the output power from the wavelength converter is reduced. For the 10-dB extinction at output wavelengths of 1533, 1545, 1555, and 1564 nm, the corresponding reverse biases required are -1.35, -1.6, -1.9, and -2.4V, and the output powers at these biases are -5.2, -2.6, -1, and -0.5 dBm, respectively.

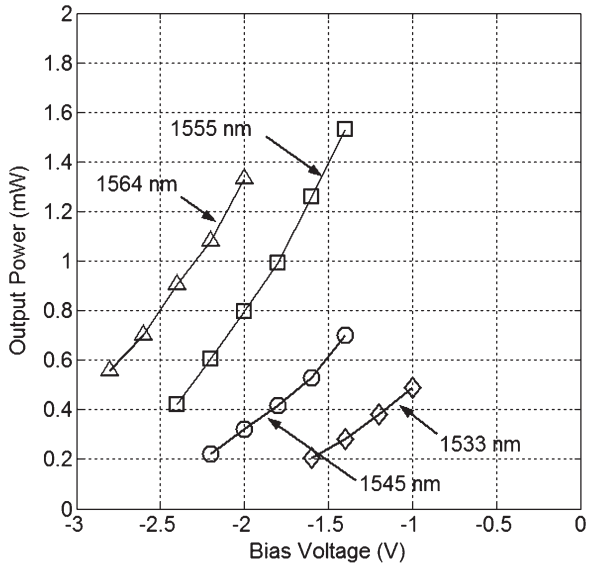

Fig. 17. Average fiber-coupled output power versus wavelength and reverse bias. The 10-dB ER bias points are -1.3, -1.7, -2.2, and -2.3 V for 1533, 1545, 1557, and 1565 nm, respectively. The input wavelength is 1548 nm, and the input power is -7 dBm.

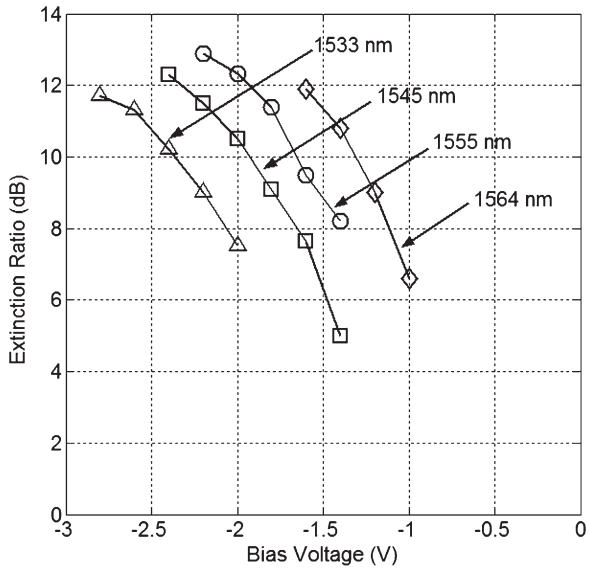

Fig. 18. Wavelength-converted ER from the PD-WC. The bias points for the 10-dB ER are -1.2, -1.6, -1.9, and -2.4 V at output wavelengths of 1533, 1545, 1557, and 1566 nm, respectively. The input wavelength is 1548 nm, and the input power is -7 dBm.

VII. Digital-System Experiments

To examine the performance of the integrated wavelength converter in a digital transmission system, a set of bit-error-rate (BER) measurements was performed using the test setup shown in Fig. 19. In the first set of measurements, the input power to the PD-WC receiver is identified, which minimizes the system power penalty for a conversion between 1548 and 1563 nm. This input power is then used to perform wavelength switching between a single input wavelength and a range of output wavelengths, followed by switching from a range of input wavelengths to a single output wavelength. The BER measurements were performed using a $2^{31} - 1$ PRBS at 10 Gb/s with nonreturn-to-zero data. The SGDBR bias conditions and receiver-amplifier bias conditions are the same, as outlined in Section VI.

The first set of BER measurements is used to identify the input power to the PD-WC that will give the minimum power penalty for wavelength switching between 1548 and 1563 nm.

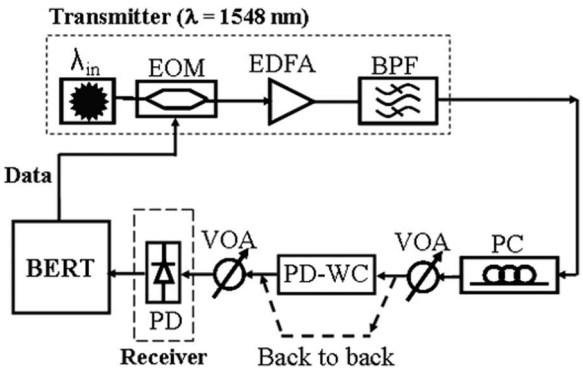

Fig. 19. Test setup used for digital-system experiments. For experiments where a nonfixed wavelength input source is used, the transmitter light source $(\lambda_{\rm in})$ is replaced with a tunable laser.

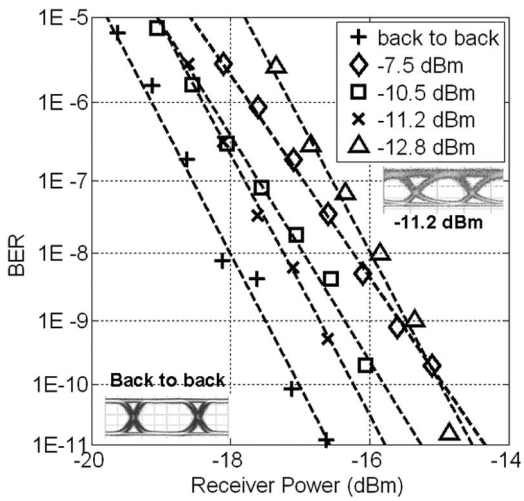

Fig. 20. Wavelength-converted and back-to-back BER measurements for various input powers at a reverse bias of −3.1 V. The input and output wavelengths are 1548 and 1563 nm, respectively.

In these experiments, a fixed reverse bias is applied to the EAM and QW p-i-n for the maximum EAM efficiency (−2.8V). The results for these BER experiments are shown in Fig. 20 for input-power levels of −7.5, −10.5, −11.2, and −12.8 dBm. The power penalty for each PD-WC input power is calculated as the difference in optical power into the external receiver that is required for a BER of 10^{-9} between the wavelength-converted signals and the signals from the transmitter in the test setup (back to back). As the power to the receiver increases from −12.8 to −11.2 dBm, the BER results show that the power penalty decreases. However, as the receiver power is increased from −11.2 to −10.5 dBm, then to −7.5 dBm, the power penalty actually increases despite an increase in the wavelength-converted signal ER. The increase in the power penalty with higher input powers is accompanied by a change in the BER slope. The change in the slope of the BER curves at higher input powers indicates a redistribution of the noise statistics through the device and most likely comes as a result of the saturation effects in the receiver preamplifier. This behavior is not necessarily unexpected as other authors have seen similar noise redistribution for preamplified receivers operating below their 1-dB gain-compression points [20]. The power penalty as a function of the input power and the wavelength-converted

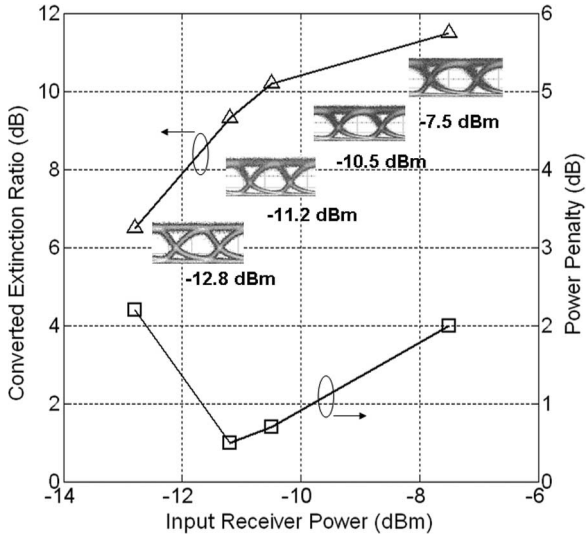

Fig. 21. Summary of wavelength-converted ER and BER power penalty along with eye diagrams from BER experiments using various receiver input powers. The input and converted wavelengths are 1548 and 1563 nm, respectively, with an applied bias of −2.8V.

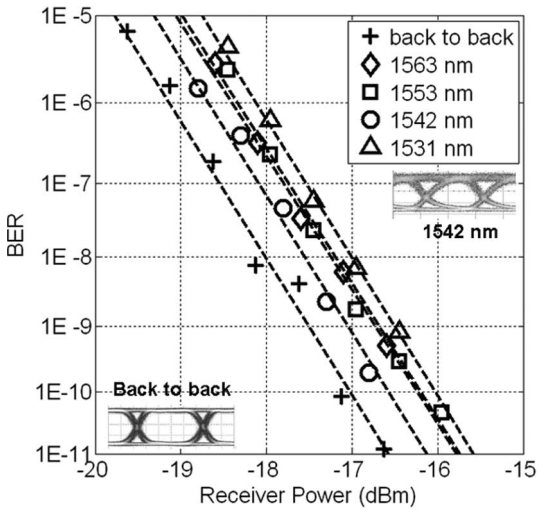

Fig. 22. BER measurement results for the PD-WC with an input power of −11 dBm and various output wavelengths. Bias conditions are adjusted to achieve 8–9-dB ER. The input wavelength is 1548 nm.

signal ER for output signals from the PD-WC are shown in Fig. 21. The figure also contains the wavelength-converted eye diagrams corresponding to each input-power level. In the eye diagrams, the additive noise on the "one" level at the higher input powers is a result of the receiver SOA gain overshoot and most likely contributes to the noise redistribution seen in the BER results in Fig. 20.

Using the optimized input-power level (−11.2 dBm), the wavelength-conversion BER experiments were performed using an input signal at 1548 nm and an output wavelength ranging from 1531 to 1564 nm. The results are shown in Fig. 22. The reverse-bias points at output wavelengths of 1563, 1553, 1542, and 1531 nm were −2.9, −2.7, −2.0, and −1.5 V, respectively, and were selected to achieve wavelength-converted ERs between 8 and 9 dB. A summary of the output extinction and output power of the device at each of these bias conditions

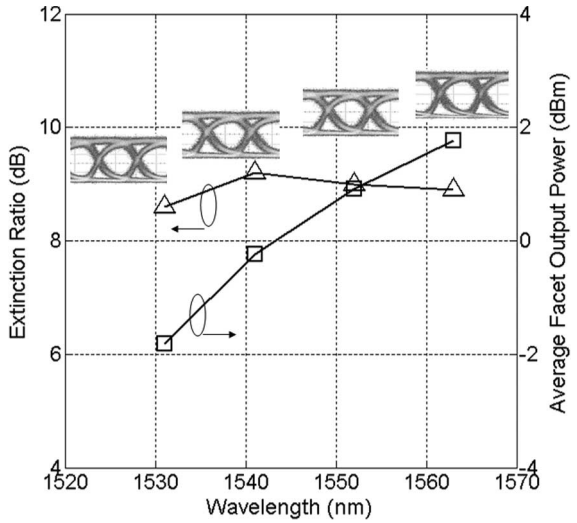

Fig. 23. Output extinction and average output facet power (fiber coupling loss removed) in BER measurements to achieve less than 1-dB power penalty for wavelength-converted signals.

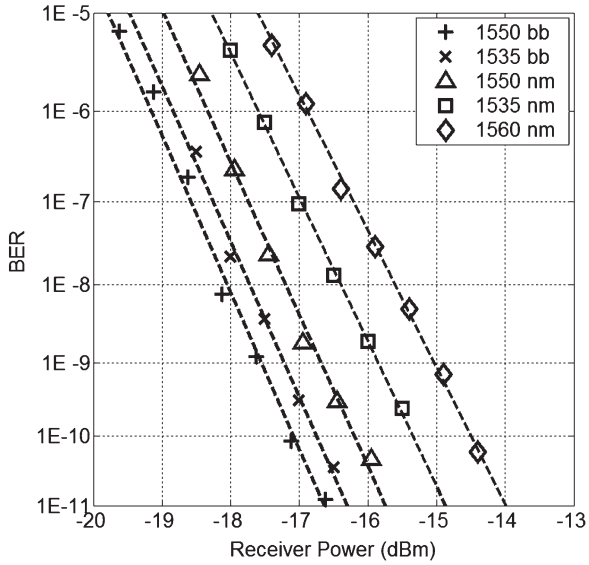

Fig. 24. BER measurement results for fixed out wavelength (1553 nm) and variable input wavelengths. The receiver power is −11 dBm for all input wavelengths, and the PD-WC reverse bias is set to achieve the maximum EAM slope efficiency.

(with the 4.2-dB fiber coupling loss removed) is shown in Fig. 23. Taking into account the input facet power of −11 dBm, this gives gains of the wavelength converter of 9, 11, 12, and 13 dBm at output wavelengths of 1531, 1542, 1553, and 1563 nm, respectively.

The remaining critical factor for broadband operation of the integrated PD-WC is the performance of the device under various input-wavelength conditions. A set of BER experiments was performed, where the input wavelength was varied between 1535 and 1560 nm and where the output wavelength was held fixed at 1553 nm. The results are shown in Fig. 24, along with the back-to-back measurements at 1530 and 1550 nm. Less than 2.5-dB power penalty is observed when the bias conditions on the PD-WC were set for the optimal extinction characteristics. The input power in each of these experiments was held fixed at −11 dBm. The ERs for output wavelengths of 1535, 1550, and 1560 nm, were 7.4, 9, and 6.5 dB, respectively. The lower ERs at input wavelengths of 1530 and 1560 nm are a result of the increase in optical loss at the low end of the wavelength spectrum shown in Fig. 5 and the decrease in optical gain as the operating wavelength moves away from the PL peak of the OQW stack.

VIII. Conclusion

We have presented a detailed study of a monolithic 10-Gb/s PD-WC that consists of a widely tunable laser source and optical receiver. The device is fabricated on a DQW integration platform and utilizes QWs for modulation efficiency in the integrated EAMs without incorporating multiple regrowth steps. The dynamic measurements of the wavelength-converted ERs show in excess of 10 dB over the full wavelength tuning range. Digital-system-performance measurements with a fixed wavelength input signal show less than 1 dB power penalty for the converted signals over output wavelengths between 1533 and 1564 nm with a facet-to-facet conversion gain between 9 and 13 dB. The BER measurements with variable input wavelengths and a fixed output wavelength show less than 2.5-dB power penalty for input wavelengths between 1535 and 1560 nm.

Acknowledgment

The authors would like to thank JDS Uniphase Corporation for the AR coatings, along with Prof. J. Bowers of the University of California—Santa Barbara and M. J. Paniccia of Intel Corporation for their support during this work.

References

[1] S. B. Yoo, "Wavelength conversion technologies for WDM network applications," *J. Lightw. Technol.*, vol. 14, no. 6, pp. 955–966, Jun. 1996.

[2] W. Idler, K. Daube, G. Laube, M. Schilling, P. Wiedemann, K. Dutting, M. Klenk, E. Lach, and K. Wunstel, "10 Gb/s wavelength conversion with integrated multiquantum-well-based 3-port Mach–Zehnder interferometer," *IEEE Photon. Technol. Lett.*, vol. 16, no. 9, pp. 1163–1165, Sep. 1998.

[3] S. Hojfeldt, S. Bischoff, and J. Mork, "All-optical wavelength conversion and signal regeneration using an electroabsorption modulator," *J. Lightw. Technol.*, vol. 18, no. 8, pp. 1121–1127, Aug. 2000.

[4] S. Kodama, T. Yoshimatsu, and H. Ito, "500 Gb/s optical gate monolithically integrated photodiode and electroabsorption modulator," *Electron. Lett.*, vol. 40, no. 9, pp. 555–556, Apr. 2004.

[5] A. Kelley, D. Marcenac, and D. Nesset, "40 Gb/s wavelength conversion over 24.6 nm using FWM in a semiconductor optical amplifier with an optimized MQW active region," *Electron. Lett.,*, vol. 33, no. 25, pp. 2123–2124, Dec. 1997.

[6] V. Lal, M. L. Masanovic, J. A. Summers, L. A. Coldren, and D. J. Blumenthal, "Performance optimization of an InP-based widely tunable all-optical wavelength converter operating at 40 Gb/s," *IEEE Photon. Technol. Lett.*, vol. 18, no. 4, pp. 577–579, Feb. 2006.

[7] J. Leuthold, P. Besse, E. Gamper, M. Dulk, S. Fisher, G. Geukos, and H. Melchior, "All-optical Mach–Zehnder interferometer wavelength converters and switches with integrated data and control signal separation scheme," *J. Lightw. Technol.*, vol. 17, no. 6, pp. 1056–1066, Jun. 1999.

[8] R. Doshi, M. L. Masanovic, and D. J. Blumenthal, "Demonstration of any λ_{in} to any λ_{out} wavelength conversion using a 2-stage all-optical wavelength converter consisting of a XGM SOA-WC and InP monolithically-integrated widely-tunable MZI SOA-WC," in *Proc. Meeting LEOS*, 2003, vol. 2, pp. 477–478.

[9] J. S. Barton, E. J. Skogen, M. L. Masanovic, J. Raring, M. N. Sysak, L. Johansson, S. P. DenBaars, and L. A. Coldren, "Photonic integrated circuits based on sampled-grating distributed-Bragg-reflector lasers," *Proc. SPIE-Int. Soc. Opt. Eng.*, vol. 4998, pp. 43–54, 2003.
[10] M. N. Sysak, J. W. Raring, J. S. Barton, H. N. Poulsen, D. J. Blumenthal, and L. A. Coldren, "Extinction ratio regeneration, signal re-amplification (2R), and broadband wavelength switching using a monolithically integrated photocurrent driven wavelength converter," *Opt. Express*, vol. 14, no. 23, pp. 11343–11348, Nov. 2006.
[11] M. N. Sysak, L. A. Johannson, J. W. Raring, H. N. Poulsen, D. J. Blumenthal, and L. A. Coldren, "Broadband return to zero (RZ) signal regeneration and broadband wavelength conversion using a monolithically integrated, photocurrent driven wavelength converter," *Electron. Lett.*, vol. 42, no. 25, pp. 1479–1481, Dec. 2006.
[12] Y. A. Akulova, G. A. Fish, H. Xu, E. Hall, M. C. Larson, P. Abraham, H. Marchand, C. Turner, C. Coldren, E. Hegblom, T. A. Strand, and L. A. Coldren, "Monolithically integrated tunable transmitters," presented at the Integrated Photonics Research and Applications (IPRA), San Diego, CA, Apr. 11–15, 2005, Paper IWF4.
[13] M. N. Sysak, J. W. Raring, J. S. Barton, M. Dummer, D. J. Blumenthal, and L. A. Coldren, "A single regrowth integration platform for photonic circuits incorporating tunable SGDBR laser and quantum well EAMs," *IEEE Photon. Technol. Lett.*, vol. 18, no. 15, pp. 1630–1632, Aug. 2006.
[14] M. N. Sysak, J. W. Raring, D. J. Blumenthal, and L. A. Coldren, "A quantum well EAM-SGDBR widely tunable transmitter fabricated in a novel dual quantum well integration platform," in *Proc. DRC, IIA-2*, Jun. 2006, pp. 15–16.
[15] J. Dow and D. Redfield, "Toward a unified theory of Urbach's rule and exponential absorption edge," *Phys. Rev. B, Condens. Matter*, vol. 5, no. 2, pp. 594–609, Jan. 1972.
[16] J. W. Raring, E. J. Skogen, C. S. Wang, J. S. Barton, G. B. Morrison, S. Demiguel, S. P. Denbaars, and L. A. Coldren, "Design and demonstration of novel QW intermixing scheme for the integration of UTC-type photodiodes with QW-based components," *IEEE J. Quantum Electron.*, vol. 42, no. 2, pp. 171–181, Feb. 2006.
[17] V. Lal, W. Donat, A. Tauke-Pedretti, L. A. Coldren, and D. J. Blumenthal, "Broadband rate-equation model including many-body gain for WDM traveling-wave SOAs," in *Proc. NUSOD*, Berlin, Germany, 2005, pp. 125–126.
[18] A. Tauke-Pedretti, M. Dummer, J. S. Barton, M. N. Sysak, J. W. Raring, and L. A. Coldren, "High saturation power and high gain integrated receivers," *IEEE Photon. Technol. Lett.*, vol. 17, no. 10, pp. 2167–2169, Oct. 2005.
[19] S. Hojfeldt and J. Mork, "Modeling of carrier dynamics in quantum-well electroabsorption modulators," *IEEE J. Sel. Topics Quantum Electron.*, vol. 8, no. 6, pp. 1265–1276, Dec. 2002.
[20] K. Morito, M. Ekawa, T. Watanabe, and Y. Kotaki, "High-output-power polarization-insensitive semiconductor optical amplifier," *J. Lightw. Technol.*, vol. 21, no. 1, pp. 176–181, Jan. 2001.

Matthew N. Sysak (M'01) was born in Smithtown, NY, in 1976. He received the B.S. degree in chemical engineering from Pennsylvania State University, University Park, in 1998 and the M.S and Ph.D. degrees in electrical and computer engineering from the University of California—Santa Barbara, in 2002 and 2005, respectively. His dissertation focused on the design and fabrication of monolithically integrated widely tunable sampled-grating distributed-Bragg-reflector semiconductor lasers, semiconductor optical amplifiers, electroabsorption modulators, and photodetectors for wavelength conversion and signal regeneration using a novel dual quantum-well integration platform.

He is currently working as a Postdoctoral Researcher with Prof. J. Bowers in the Ultrafast Optoelectronics Group, Department of Electrical and Computer Engineering, University of California—Santa Barbara, focusing on the design and fabrication of ultralinear monolithically integrated photonic links.

Dr. Sysak is a member of the Optical Society of America and The International Society for Optical Engineers.

James W. Raring (M'01) received the B.S. degree from California Polytechnic State University, San Luis Obispo, in 2001 and the Ph.D. degree in materials science from the University of California, Santa Barbara, in 2006. His Ph.D. research focused on the design, growth, and fabrication of high-functionality wavelength-agile InGaAsP-based photonic integrated circuits (PICs). By coupling quantum well intermixing with MOCVD regrowth, he combined widely tunable sampled grating DBR lasers, 40-Gb/s electroabsorption modulators, low-confinement high-saturation power semiconductor optical amplifiers, and 40-Gb/s unitraveling carrier photodiodes to demonstrate the first single-chip 40-Gb/s optical transceiver.

In 2006, he joined the RF/Optoelectronic Group, Sandia National Laboratories, Albuquerque, NM, where he is currently working on leading edge PICs. He is the author or coauthor of more than 75 technical papers.

Dr. Raring is a member of the IEEE Lasers and Electro-Optics Society, the Optical Society of America, and the International Society for Optical Engineers.

Jonathon S. Barton (S'97–M'98) received the B.S. degree in electrical engineering and material science from the University of California—Davis in 1997 and the Ph.D. degree in electronic materials from the University of California—Santa Barbara.

He was an Intel Fellow during the time he received his doctorate. Currently, he is an Assistant Project Scientist for the Laser Switched Optical Router Defense Advanced Research Projects Agency grant, working on the growth, fabrication, and high-speed testing of many monolithic optoelectronic components such as tunable lasers, modulators, and photocurrent-driven wavelength converters. He is also currently with the Department of Materials, University of California—Santa Barbara.

Dr. Barton is a member of the IEEE Lasers and Electro-Optics Society, the Optical Society of America, and The International Society for Optical Engineers.

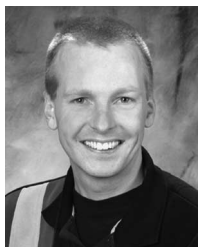

Henrik N. Poulsen received the M.Sc.E.E. degree from the Technical University of Denmark, Lyngby, Denmark, in 1995.

From 1995 to 2001, he first worked as a Research Associate and later as an Associate Research Professor in the field of high-speed wavelength-division multiplexing and optical time-division multiplexing. In 2001, he moved from Copenhagen, Denmark, to Santa Barbara, CA, to join Calient Networks, where he worked on optical amplification and performance monitoring for all-optical microelectromechanical-system-based switches. He is currently working as an Associate Project Scientist with Prof. D. J. Blumenthal in the Optical Communications and Photonics Network Group, Department of Electrical and Computer Engineering, University of California—Santa Barbara. His main research area is all-optical packet switching using all-optical interferometric structures. His main interests were ultrahigh-speed optical signal processing using nonlinear fiber and semiconductor materials, mainly semiconductor optical amplifiers, interferometric structures, and electroabsorption modulators.

Daniel J. Blumenthal (S'91–M'93–SM'97–F'03) received the B.S.E.E. degree from the University of Rochester, Rochester, NY, in 1981, the M.S.E.E. degree from Columbia University, New York, NY, in 1988, and the Ph.D. degree from the University of Colorado at Boulder, Boulder, in 1993.

In 1981, he was with the StorageTek, Louisville, CO, in the area of optical data storage. In 1986, he was with Columbia University in the areas of photonic switching systems, ultrafast all-optical networks, and signal processing. From 1993 to 1997, he was an Assistant Professor with the School of Electrical and Computer Engineering, Georgia Institute of Technology, Atlanta. He is currently a Professor with the Department of Electrical and Computer Engineering, University of California—Santa Barbara, and the Associate Director for the Center on Multidisciplinary Optical Switching Technology. He heads the Optical Communications and Photonic Networks Research. He is the Cofounder of Calient Networks, a manufacturer of photonic switching systems, which is based in San Jose, CA. His current research areas are in optical communications, wavelength-division multiplexing, photonic packet-switched and all-optical networks, all-optical wavelength conversion, and optical subcarrier multiplexing. He has authored or coauthored over 100 papers in these and related areas.

Dr. Blumenthal is a member of the Optical Society of America. He is the recipient of the 1999 Presidential Early Career Award for Scientists and Engineers, the 1994 National Science Foundation Young Investigator Award, and the 1997 Office of Naval Research Young Investigator Program Award. He served as an Associate Editor for the IEEE PHOTONICS TECHNOLOGY LETTERS and the IEEE TRANSACTIONS ON COMMUNICATIONS. He was a Guest Editor for the IEEE JOURNAL OF LIGHTWAVE TECHNOLOGY *Special Issue in Photonic Packet Switching Systems, Technologies, and Techniques*, which was published in December 1998. He also served as the Program Chair and the Technical Program Committee member on numerous conferences.

Larry A. Coldren (S'67–M'72–SM'77–F'82) received the Ph.D. degree in electrical engineering from Stanford University, Stanford, CA, in 1972.

He is the Fred Kavli Professor of optoelectronics and sensors with the University of California—Santa Barbara (UCSB). He is also the Chairman and Chief Technology Officer of Agility Communications, Inc. After 13 years in the research area at Bell Laboratories, Murray Hill, NJ, he has been with the UCSB since 1984, where he now holds appointments in the Departments of Materials and Electrical and Computer Engineering and is the Director of the Optoelectronics Technology Center. In 1990, he cofounded Optical Concepts, later acquired as Gore Photonics, to develop novel vertical-cavity surface-emitting laser (VCSEL) technology, and in 1998, he cofounded Agility Communications, Inc. to develop widely tunable integrated transmitters. At Bell Labs, he initially worked on waveguided surface-acoustic-wave signal-processing devices and coupled-resonator filters. He later developed tunable coupled-cavity lasers using novel reactive-ion-etching technology that he created for the then new InP-based materials. At the UCSB, he continued working on multiple-section tunable lasers; in 1988, he invented the widely tunable multielement mirror concept, which is now fundamental to many of Agility's products. During the late 1980s, he also developed efficient vertical-cavity multiple-quantum-well modulators, which led to the novel VCSEL designs that provided unparalleled levels of performance. He continues to be active in developing new photonic integrated circuit (PIC) and VCSEL technology, including the underlying materials growth and fabrication techniques. In recent years, for example, he has been involved in the creation of vertical and in-plane GaN-based emitters, efficient all-epitaxial InP-based VCSELs, and a variety of PICs incorporating numerous optical elements for widely tunable integrated transmitters, receivers, and wavelength converters. He has authored or coauthored over 700 papers, five book chapters, and one textbook and is the holder of 36 patents.

Dr. Coldren is a fellow of the Optical Society of America and the Institution of Electrical Engineers and a member of the National Academy of Engineering. He is the recipient of the 2004 John Tyndall Award. He has presented dozens of invited and plenary talks at major conferences.